

Non-prehensile Planar Manipulation via Trajectory Optimization with Complementarity Constraints

João Moura^{1,2}, Theodoros Stouraitis¹, and Sethu Vijayakumar^{1,2}

Abstract—Contact adaptation is an essential capability when manipulating objects. Two key contact modes of non-prehensile manipulation are sticking and sliding. This paper presents a Trajectory Optimization (TO) method formulated as a Mathematical Program with Complementarity Constraints (MPCC), which is able to switch between these two modes. We show that this formulation can be applicable to both planning and Model Predictive Control (MPC) for planar manipulation tasks. We numerically compare: (i) our planner against a mixed integer alternative, showing that the MPCC planner converges faster, scales better with respect to the time horizon (TH), and can handle environments with obstacles; (ii) our controller against a state-of-the-art mixed integer approach, showing that the MPCC controller achieves improved tracking and more consistent computation times. Additionally, we experimentally validate both our planner and controller with the KUKA LWR robot on a range of planar manipulation tasks. See our accompanying video here: <https://youtu.be/EkU6YHMhjt0>.

I. INTRODUCTION

Moving beyond the typical pick-and-place tasks, towards non-prehensile manipulation, requires providing robots with the capability of adapting contact locations on the object. However, achieving reliable robot manipulation via contact adaptation still poses many challenges due to, among other factors: (a) the under-actuated and hybrid nature of the problem [1], [2]; and (b) the uncertainties arising from the frictional contact interactions [3], [4]. Recent works [5]–[7] have been addressing the problem of contact adaptation by developing control and motion planning methods based on Trajectory Optimization (TO) that explicitly incorporate models of the contact interaction. Nevertheless, there are still many open questions on both making plans with complex contact interactions [8] realizable by robots and expanding the capabilities of current contact-aware controllers [5], [9] to reliably handle more challenging environments.

A. Related Work

Non-prehensile manipulation, a term introduced by Mason [10], refers to manipulation without grasping, *i.e.* the relative pose between the object and the robots' end-effectors can change throughout the interaction. While that type of manipulation can allow robots to execute a wider range of tasks [1], executing such tasks with robots can prove itself quite challenging, in part due to various mismatches between the physical world and the respective models used for planning and control. One prominent and widely used task, also



Fig. 1. Experimental setup where the robot plans and controls the motion of an object to push it to the target, via sliding contact and while avoiding an obstacle.

introduced by Mason [1], for studying non-prehensile manipulation is the planar pusher-slider example. This example, as shown in Fig. 1, consists of a flat object—the slider—moving on a planar surface, pushed by the end-effector of the robot—the pusher. The pusher-slider example is especially useful for exploring concepts such as the limit-surface model [11], the motion cone concept [1], its generalization to a broader set of planar tasks [12], tactile feedback [13], and dynamics learning [4], [14]. Recently, Hogan and Rodriguez [2] proposed a Model Predictive Controller (MPC) for reactive tracking of nominal paths while reacting to disturbances. They incorporate the selection of different contact modes, such as sticking and sliding contact, in the MPC optimization by using a mixed integer formulation. In this work, we investigate the limitations of this formulation in the context of both control and planning of planar sliding motions.

Recent works [6], [15]–[17] have developed TO methods for planning robot manipulation tasks requiring contact changes. The underlying formulation of these works follows one of two classes: *contact-implicit* [18] or *multi-mode* [6], [19]. Here, we focus on the former which expresses the hybrid nature of the contact change as a Mathematical Program with Complementarity Constraints (MPCC). For the problem of making and breaking of contact, the complementarity constraint typically takes the form of $0 \leq d \perp f \geq 0$, where d and f are, respectively, the distance and the normal force between two objects of interest. This constraint enforces both unilateral forces and that there is no penetration, while encoding the hybrid condition that the objects are either in contact or apart having, respectively, zero distance or zero contact force between them. To the extend of our knowledge no work has demonstrated the application of MPCC for robot

¹ Authors are with the School of Informatics, The University of Edinburgh, Edinburgh, U.K.

² Authors are with The Alan Turing Institute, London, U.K.

control problems, due to its computational requirements, yet we show that it is a particularly well suited formulation for both planning and control of planar non-prehensile manipulation problems with sticking and sliding contacts.

B. Problem Statement

In the Related Work we discuss a control formulation that explicitly handles switching contact modes, which requires high level methods to provide nominal paths. There are a number of TO works capable of generating those nominal hybrid motion paths, *i.e.* involving change of contacts, however, realizing these on hardware is still a subject of research. Hence, we ask ourselves “*what is an appropriate numerical optimal control formulation for non-prehensile manipulation problems with sliding contact that is applicable to both control and planning problems?*” As a typical example scenario, consider a robot pushing an object to a goal, as shown in Fig. 1. In such a case, the robot needs to address the following challenges:

- It has to plan a trajectory using both sticking and sliding contact modes to drive the object to the target while avoiding the obstacle;
- It has to control the motion of the object to track the planned trajectory under the uncertainties of the frictional contact interactions and other unknown disturbances.

Contributions: This work addresses these challenges, by:

- Proposing a single MPCC formulation for both planning and control (MPC) that enables switching between sticking and sliding contact modes;
- Comparing it numerically with an alternative mixed integer formulation, showing that the MPCC achieves i) smaller tracking errors, ii) more reliable computation times under large disturbances, iii) and better scalability with regards to the time horizon (TH) and to a broader range of problems, *e.g.* problems with obstacles;
- And finally, experimentally validating our MPCC formulation using the KUKA LWR robot hardware.

II. BACKGROUND

This section revises three key models/assumptions commonly used in the literature for modelling the planar pusher-slider system. Namely, the quasi-static assumption, the limit surface, and the friction cone.

A. System Description

Fig. 2 illustrates a top down view of the planar pusher-slider system, where $(^G x_S, ^G y_S)$ and θ are, respectively, the Cartesian position and orientation of the sliding object—the slider—with respect to a global reference G . Given a known geometry of the slider $r(\phi)$, a single parameter ϕ_C is sufficient to compute the position of the pushing object—the pusher—as well as the contact point C , normal n and tangential t directions.

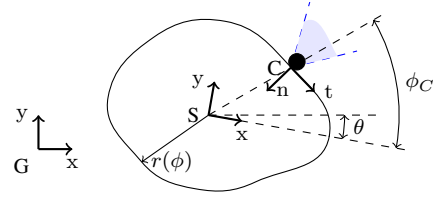


Fig. 2. Illustration of the pusher-slider system.

B. Quasi-static Assumption

Let $\omega = [v_x, v_y, \omega_z]^T$ and $\tau = [f_x, f_y, \tau_z]^T$ be, respectively, the vectors of generalized velocities and forces for the slider. Then we can write its Newtonian dynamics as

$$I\dot{\omega} = \tau_C + \tau_P, \quad (1)$$

where I is the inertia matrix of the slider, τ_C are the forces due to lateral contacts (pusher) and τ_P are the forces due to the sliding friction with the planar surface. However, it is common practice in the literature to simplify the equation of motion (1), by neglecting the inertial forces $I\dot{\omega}$, based on the observation that for low velocities ω , frictional contact forces dominate the motion dynamics of the pusher-slider system [1]. Thus, we obtain $\tau_C = -\tau_P$.

C. Ellipsoidal Approximation of the Limit Surface

Now, we need to find a model for computing the friction forces τ_P . Goyal *et al.* [11] introduced the idea of limit surface that describes the mapping between τ_P and ω . In this work, we use the following ellipsoidal approximation to model the limit surface

$$H(\tau_P) \triangleq \tau_P^T L \tau_P, \quad (2)$$

where L is a positive definite matrix [14]. This model captures well the shape of the limit surface for pusher-slider interactions with uniform pressure distributions [20]. Given a convex limit surface $H(\tau_P)$, the slider velocities will be perpendicular to the limit surface [2], resulting in

$$\omega = \nabla H(\tau_P) = L \tau_P. \quad (3)$$

D. Motion Model

This subsection describes the motion model used to predict and optimize the motion of the pusher-slider system. Given the quasi-static assumption, the motion model becomes a geometric kinematic model and, hence, the state simply corresponds to the system configuration

$$x = [^G x_S, ^G y_S, \theta, \phi_C]^T, \quad (4)$$

which describes the position and orientation of the pusher and slider. A possible representation for the control is

$$u = [f_n, f_t, \dot{\phi}_{C+}, \dot{\phi}_{C-}]^T, \quad (5)$$

where f_n and f_t are, respectively, the normal and tangential forces applied by the pusher to the slider, and $\dot{\phi}_C = \dot{\phi}_{C+} - \dot{\phi}_{C-}$ is the angular rate of sliding. Note that (5) is a redundant representation that we will discuss in the next subsection.

For single contact and a rectangular object with contact C and local S frames aligned, through simple geometric

transformations, using the ellipsoidal approximation of the limit surface (3), and the quasi-static assumption, we obtain the following equations of motion for the pusher-slider system [2]

$$\dot{x} = f(x, u) = \begin{bmatrix} RLJ_C^\top & 0 & 0 \\ 0 & 1 & -1 \end{bmatrix} u, \quad (6)$$

with $R(\theta)$ being the xy-plane rotation matrix between the slider local frame S and the global frame G , and

$$J_C = \begin{bmatrix} 1 & 0 & -s_{y_C} \\ 0 & 1 & s_{x_C} \end{bmatrix}$$

being the contact Jacobian matrix.

E. Friction Constraints

Depending on the values that the redundant set of controls in (5) take, the pusher-slider system can exhibit different dynamic behaviours. Those different behaviours, or dynamic modes, include sticking or sliding contact between the pusher and the slider, or even no contact at all. Originally, Hogan and Rodriguez [21] proposed a hybrid dynamics model for the equations of motion $f(\cdot)$. Later, they [2] expressed the hybrid nature of the system via constraints on the controls (5). In that way, they separate the continuous dynamics of the system, as in (6), from the hybrid component corresponding to different active contact modes. The advantage of this approach, in the context of formulating an optimization, is the ease of transcribing the selection of contact modes, hence, we stick with this approach.

Regardless of the active contact mode, we enforce a unilateral constraint that allows only pushing of the slider, as $\mathcal{U}_0 : f_n \geq 0$. Fig. 3 illustrates the three contact modes considered, corresponding to the following sets of constraints

$$\mathcal{U}_1 : \begin{cases} \dot{\phi}_C = 0 \\ |f_t| \leq \mu f_n \end{cases}, \mathcal{U}_2 : \begin{cases} \dot{\phi}_C > 0 \\ f_t = \mu f_n \end{cases}, \text{ and } \mathcal{U}_3 : \begin{cases} \dot{\phi}_C < 0 \\ f_t = -\mu f_n \end{cases}.$$

For a sticking contact, corresponding to \mathcal{U}_1 and illustrated by Fig. 3a, the applied force has to remain within the friction cone and the angular rate of sliding $\dot{\phi}_C$ has to be zero. Note that μ is the friction coefficient between the pusher and the slider. For the sliding counterclockwise (ccw) contact mode, corresponding to \mathcal{U}_2 and illustrated by Fig. 3b, the applied force belongs to the one edge of the friction cone while $\dot{\phi}_C$ is positive. Finally, for the clockwise (cw) contact mode, corresponding to \mathcal{U}_3 and illustrated by Fig. 3c, the applied force belongs to the other edge of the friction cone while $\dot{\phi}_C$ is negative.

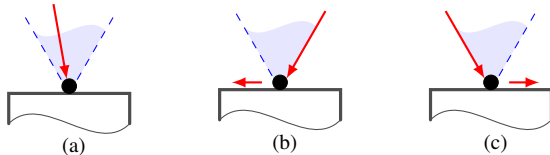


Fig. 3. Slider contact modes: (a) sticking; (b) sliding counterclockwise (ccw); (c) sliding clockwise (cw).

III. METHOD

A. Mixed Integer Formulation

When developing an optimal control formulation for computing trajectories for the pusher-slider system that is hybrid, a natural way of incorporating contact modes switching is to include one binary variable z per contact mode defining what mode is active at any instance of time. Following this, we can then formalize a Trajectory Optimization (TO) Mixed Integer Non-Linear Program (MINLP) as follows

$$\min_{x_i, u_i, z_i} C(x_{0:N}, u_{0:N-1}, z_{1:3,0:N-1}) \quad (7a)$$

$$\text{subject to } x_{i+1} = x_i + \Delta t f(x_i, u_i), x_i \in \mathcal{X}, \quad (7b)$$

$$u_i \in \mathcal{U}_0 \text{ (unilaterality)}, \quad (7c)$$

$$u_i \in \mathcal{U}_1 \text{ if } z_{1,i} = 1 \text{ (sticking)}, \quad (7d)$$

$$u_i \in \mathcal{U}_2 \text{ if } z_{2,i} = 1 \text{ (sliding ccw)}, \quad (7e)$$

$$u_i \in \mathcal{U}_3 \text{ if } z_{3,i} = 1 \text{ (sliding cw)}, \quad (7f)$$

$$z_{1,i} + z_{2,i} + z_{3,i} = 1, \quad (7g)$$

where \mathcal{X} is the set of feasible states, including state bounds and obstacles, and i denotes the index of the knot, i.e. the discretization points of the transcribed problem. The cost function is $C(x_{0:N}, u_{0:N-1}, z_{1:3,0:N-1}) = \bar{x}_N^\top W_{x_N} \bar{x}_N + \sum_{i=0}^{N-1} (\bar{x}_{i+1}^\top W_x \bar{x}_{i+1} + \bar{u}_i^\top W_u \bar{u}_i + \sum_{j=1}^3 w_z z_{j,i})$, where $\bar{x}_i = x_i - x_i^*$ is the difference between the state x_i and the goal state x_i^* . We implement (7d), (7e), and (7f) through the big M formulation [22].

The MINLP in (7) is inspired by the Mixed Integer Quadratic Programming (MIQP) proposed by Hogan and Rodriguez [2]. The key difference is that the formulation in [2] requires linearization along a given nominal path (states and actions). The MIQP is a suitable formulation for control because quadratic programs are generally very fast to solve. However, it is unsuitable for planning, i.e. generating trajectories, as it requires both nominal states and actions as reference, and mixed integer programs tend to scale badly due to the combinatorial expansion when exploring the solution space of the integer variables.

B. Complementary Constraints

Another way of expressing different modes in hybrid systems is to use complementarity constraints, which have recently been widely used in many TO based planning methods for robotics [8], [9], [17], [18]. The complementarity constraints remove the need of using integer variables in the optimization problem. Particular to the pusher-slider problem, the key insight for exploring complementarity constraints instead of a mixed integer formulation is that, even though the dynamics are hybrid, the transition between the different modes is continuous, meaning that the system can transition from the currently active contact mode to any other contact mode, at any instant in time. Note that for the scenario of making and breaking of contact [8], [17], [18], when far away from contact it is physically infeasible to instantaneously transition to contact. This additional guard condition ensuring that mode transitions only occur from certain state space regions is nonexistent in our problem.

Let us introduce a vector of two variables that correspond to the edge of the friction cone

$$\lambda_v \triangleq [\lambda_-, \lambda_+]^\top \triangleq [\mu f_n - f_t, \mu f_n + f_t]^\top. \quad (8)$$

It is straightforward to show that the second inequality in \mathcal{U}_1 corresponds to having $\lambda_-, \lambda_+ \geq 0$. We also introduced the control variables $\dot{\phi}_{C+}, \dot{\phi}_{C-}$ in (5) rather than using $\dot{\phi}_C = \dot{\phi}_{C+} - \dot{\phi}_{C-}$, as in [2], to enable the formulation of the complementarity constraint. In this way, we can obtain: the sticking contact mode when both $\dot{\phi}_{C+}, \dot{\phi}_{C-} = 0$ and $\lambda_-, \lambda_+ \geq 0$; the sliding ccw contact mode \mathcal{U}_2 when both $\dot{\phi}_{C-}, \lambda_- = 0$ and $\dot{\phi}_{C+} \geq 0$; and the sliding cw contact mode \mathcal{U}_3 when both $\dot{\phi}_{C+}, \lambda_+ = 0$ and $\dot{\phi}_{C-} \geq 0$.

By defining the vector $\dot{\phi}_v \triangleq [\dot{\phi}_{C+}, \dot{\phi}_{C-}]^\top$, we can easily verify that the complementarity constraint condition $\lambda_v^\top \dot{\phi}_v = 0$, with $\dot{\phi}_{C+}, \dot{\phi}_{C-}, \lambda_-, \lambda_+ \geq 0$, simultaneously satisfies all the constraints required by the three contact modes. Therefore, we can define the complementarity constraints as

$$\mathcal{U}_{cc} : \begin{cases} \dot{\phi}_{C+}, \dot{\phi}_{C-}, \lambda_-, \lambda_+ \geq 0 \\ \lambda_v^\top \dot{\phi}_v + \varepsilon = 0 \end{cases}, \quad (9)$$

where we introduce a slack variable ε . This variable will be zero when the contact mode constraints are fully satisfied. We introduce this variable because it is well known in the literature that problems with complementarity constraints are in practise difficult to solve, usually requiring relaxations [23].

C. Non-Linear Programming (NLP)

We can then formalize our TO Mathematical Program with Complementarity Constraints (MPCC) as follows

$$\min_{x_i, u_i, \varepsilon_i} C(x_{0:N}, u_{0:N-1}, \varepsilon_{0:N-1}) \quad (10a)$$

$$\text{subject to } x_{i+1} = x_i + \Delta t f(x_i, u_i), x_i \in \mathcal{X}, \quad (10b)$$

$$u_i \in \mathcal{U}_0 \text{ (unilaterality)}, \quad (10c)$$

$$u_i, \varepsilon_i \in \mathcal{U}_{cc} \text{ (complementarity)}, \quad (10d)$$

where the cost function is $C(x_{0:N}, u_{0:N-1}, \varepsilon_{0:N-1}) = \bar{x}_N^\top W_{x_N} \bar{x}_N + \sum_{i=0}^{N-1} (\bar{x}_{i+1}^\top W_x \bar{x}_{i+1} + u_i^\top W_u u_i + w_{\varepsilon_i} \varepsilon_i^2)$. Changing formulation (10) from a tracking to a planning problem is simply a matter of specifying the full nominal state trajectory $x_{0:N}^*$ or specifying the final state target x_N^* , respectively. Also, using (10) for planning full trajectories or as a Model Predictive Controller (MPC) is also a matter of changing the horizon N , such that for a small enough horizon we can solve (10) online in a control loop.

IV. EXPERIMENTS AND RESULTS

This section presents numerical and robot experiments performed using the MPCC formulation given in (10). We compare the MPCC formulation against MIQP [2] for tracking trajectories, and against MINLP given in (7) for planning trajectories. We implemented all optimization using CasADi [24]. We used the Knitro solver [25] for both the MPCC and MINLP problems and the Gurobi solver [26] for the MIQP. We ran all the computations in a 64-bit Intel 16-Core i9 3.60GHz workstation with 64GB RAM.

For every experiment, the cost function gain matrices are $W_x = \text{diag}(1, 1, 0.01, 0.001)$, $W_u = 10^{-2} \text{diag}(1, 1, 0, 0)$, and $W_{x_N} = 10W_x$. Note that planning problems only have a single state target x_N^* , hence we only use W_{x_N} . For the mixed integer formulations $w_z = 0$. For the MPCC formulation $w_{\varepsilon_i} = 50$ for the planning problems while for the tracking problems $w_{\varepsilon_i} = 50$ for the first knot reducing exponentially to 0.1 for the last knot. The number of discretization steps of the MPC is 25 steps with $\Delta t = 1/25$ s, which results in total TH of $T = 1$ s. We use a friction coefficient of $\mu = 0.2$ for the numerical experiments and $\mu = 0.1$ for the robot experiments. We compute L in (3) according to [2].

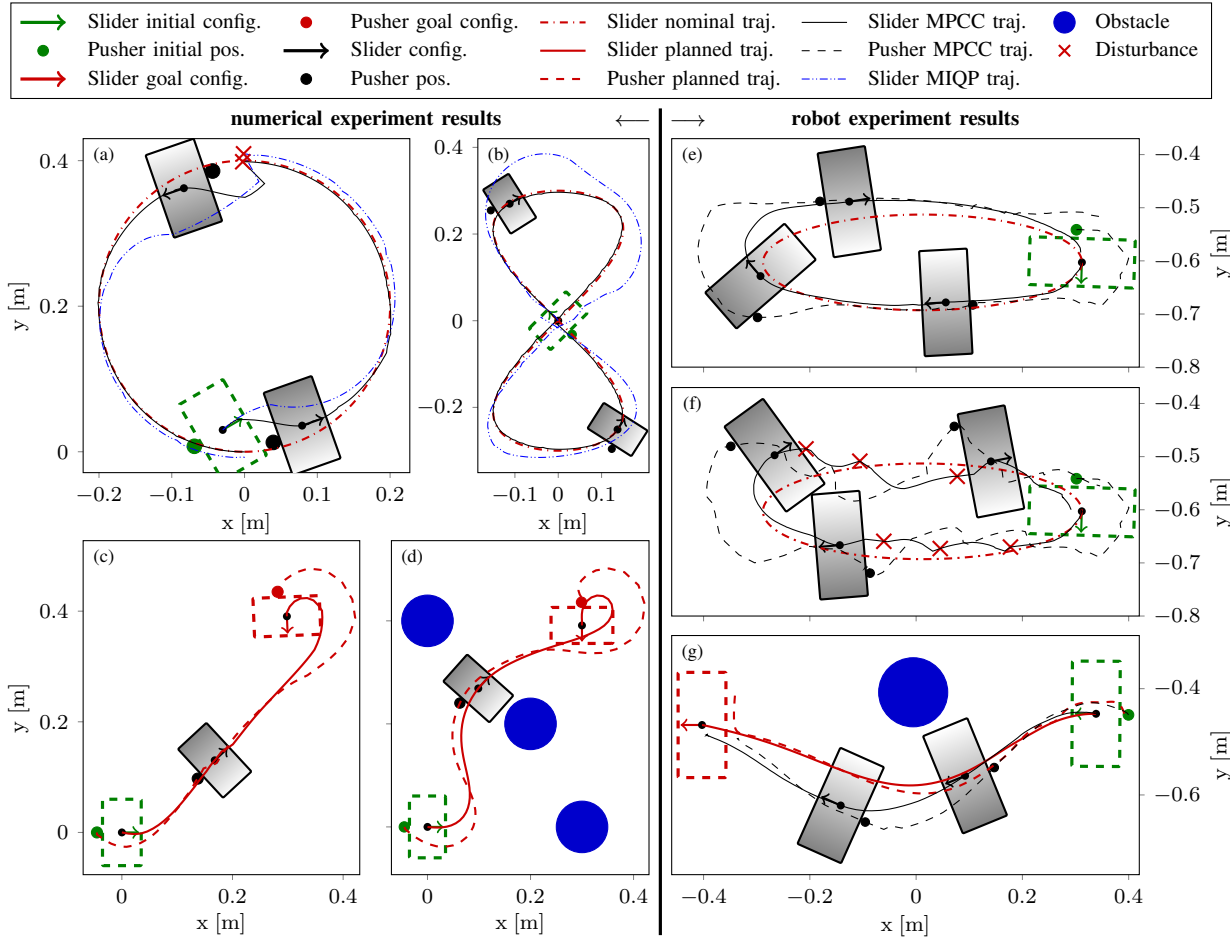
For the actual robot experiments, the MPC runs in a 50 Hz control loop. In each MPC loop, we measure the position and orientation of the slider through a VICON tracking system to generate the initial state x_0 . We then run the optimization (10) and only make use of the first state x_1 of the solution trajectory, from which we compute the position of the pusher and, through standard inverse kinematics, the respective configuration of the robot. The accompanying video shows the robot experiments detailed in this section.

A. Numerical Experiments — Tracking Nominal Trajectory

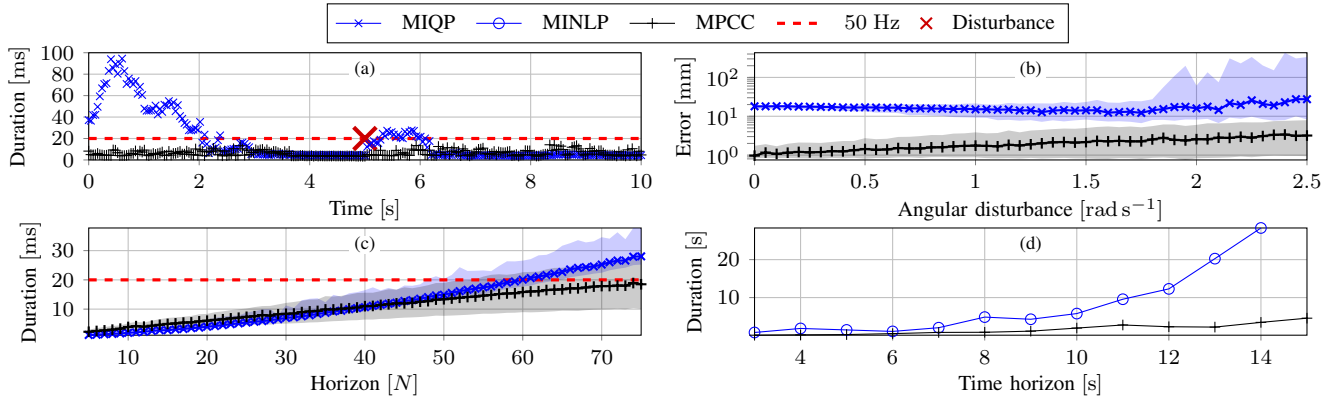
This experiment investigates the feasibility of the proposed MPCC formulation for tracking in an MPC loop. We compare the MPCC against the MIQP [2], for the task of tracking two different pre-specified nominal trajectories, a circular and an eight-shaped one. We generate pairs of nominal states and actions, which is a requirement from the MIQP (the MPCC only requires nominal states), for a pushing motion with a sticking contact. Both nominal trajectories have a total duration of 10 s with sampling times of $\Delta t = 1/25$ s. The sliding object is rectangular with dimensions 7×12 cm and the pusher has a radius of 1 cm.

Fig. 4a shows the tracking of the circular trajectory. We offset the initial state to $x_0 = [-0.03 \text{ m}, 0.03 \text{ m}, 30^\circ, 0]^\top$ and at the 5th second introduce a disturbance of $\Delta x = [0.03 \text{ m}, -0.03 \text{ m}, 30^\circ, 0]^\top$. Both MPCC and MIQP formulations are able to track the nominal trajectory, however the MPCC recovers quicker after both the initial state offset and the disturbance. Fig. 5a shows the computation times for this experiment. In the absence of disturbances both methods are able to compute solutions faster than 20 ms (> 50 Hz). However, when large deviations from the nominal trajectory occur the MIQP computation time increases significantly—rendering this method inappropriate for online use with large disturbances. Additionally, we noticed that MIQP easily becomes unstable under larger disturbances unlike the MPCC.

Furthermore, we compare the MPCC and the MIQP controllers for multiple runs on the circular trajectory when subject to angular disturbances, but without initial state offset. In this experiment, we add a disturbance to the dynamics (6) as $\dot{x} = f + \epsilon$, where $\epsilon = [0, 0, \epsilon_\theta, 0]^\top$ and we draw $\epsilon_\theta \sim \mathcal{U}(-\omega_M, \omega_M)$ from an uniform distribution. Fig. 5b shows the evolution of the position trajectory error, computed as the distance between each point of the actual



Trajectory plots for the tasks of: (a) tracking a circular trajectory; (b) tracking an eight-shaped trajectory; (c) planning a trajectory to a target; (d) planning a trajectory to a target in the presence of obstacles; (e) tracking an ellipsoidal trajectory with the robot; (f) tracking an ellipsoidal trajectory with the robot in the presence of disturbances; (g) planning and tracking a trajectory to a target with the robot in the presence of an obstacle.



Result plots of the: (a) solving time while tracking a circular trajectory; (b) trajectory tracking error when subject to angular disturbances, where we use a log scale for the vertical axis; (c) computation time of solving the MPC problem for different horizons; (d) average solving time, over five runs, for planning the path to a given goal, as shown in Fig. 4c—where for $T = 15$ s, the computation time of MINLP takes several minutes. Note that (b-c) result from tracking the circular trajectory in Fig. 4a ten times, corresponding to running the MPC loop 2500 times per value in the horizontal axis, where the line corresponds to the median and the shaded area to the 10th and the 90th percentiles.

and the nominal trajectories, for increasing ω_M , where for each value of ω_M we ran both controllers for tracking ten full circles, equating to a total of 2500 MPC loops. Fig. 5b shows that the MPCC results in a significant lower tracking error. For the same experiment, but now with a constant $\omega_M = 1.5 \text{ rad s}^{-1}$, we vary the horizon N , and compute the MPC

computation time. Fig. 5c shows that the MPCC scales better.

Fig. 4b shows the tracking of the eight-shaped trajectory, showing that the MPCC achieves qualitatively better tracking than the MIQP. Note that the MIQP linearises the dynamics along the nominal states and actions, which makes its tracking quality highly depend on the accuracy of the nominal

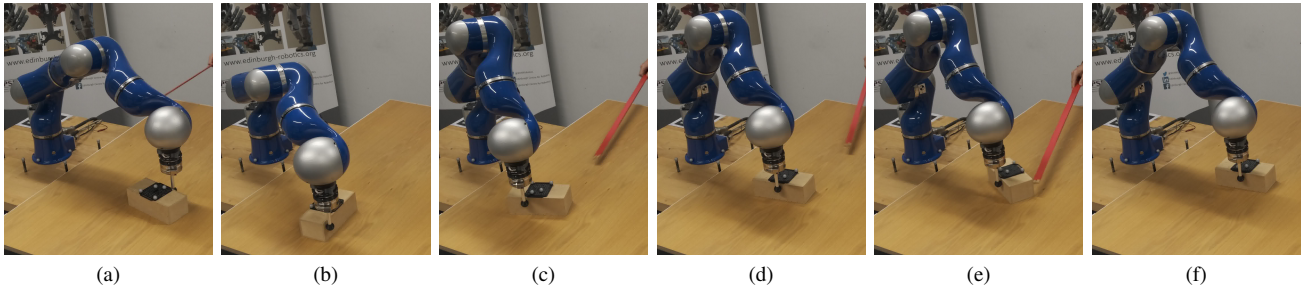


Fig. 6. Keyframes of the KUKA LWR robot tracking an ellipsoidal trajectory, where (a-c) show the sliding of the object along an aggressive curvature segment of the trajectory, and (d-f) exhibit the MPC recovering from a disturbance.

state and action pairs. However, obtaining accurate nominal actions in scenarios with aggressive curvature, like the one shown in Fig. 4b, is often unachievable. In contrast to MIQP, the MPCC dispenses with both the linearization and the nominal actions, which might explain its improved tracking.

B. Numerical Experiments — Planning

In this experiment, we test the capabilities of the MPCC formulation to generate trajectories by exploiting sticking and sliding contact modes. These trajectories drive the sliding object from an initial state to a desired target state—even in the presence of obstacles. We compare the MPCC formulation against the MINLP, see (7), both in terms of convergence and computation time. The planning tasks have as initial state $x_0 = [0, 0, 0, 0]^\top$ and as target state $x_N^* = [0.3 \text{ m}, 0.4 \text{ m}, 270^\circ, 0]^\top$. For the scenario with the obstacles each obstacle has a radius of 5 mm. We encode the obstacles in (10) as inequality constraints on the distance between the obstacle and the center of the sliding object.

Fig. 4c shows an example of a trajectory generated for a TH of $T = 3 \text{ s}$. Additionally, we generated trajectories for the same task but with varying TH, from 3 s to 15 s. Fig. 5d shows the respective computation times, showing that the MPCC takes significantly less time than the MINLP to converge and scales well with respect to the TH. Furthermore, for the scenario including obstacles, the MINLP always failed to converge to a solution, while the MPCC was able to produce plans, like the one shown in Fig. 4d. Note, however, that the MPCC optimization was able to produce planning solutions at the cost of non zero values for the complementarity slack variables, unlike the case when using MPCC for tracking with MPC, which always gave solutions with zero slack.

C. Robot Experiment — Tracking Nominal Trajectory

In this experiment, we used the KUKA LWR robot to assess our MPC implementation of the MPCC formulation for the task of tracking an ellipsoidal trajectory. The radius of the pusher is 16 mm and the size of the box is $9 \times 20 \text{ cm}$.

Fig. 4e and 4f depict two tracking experiments, one without and one with disturbances, respectively. Fig. 6 shows a sequence of images of the robot tracking the ellipsoidal trajectory, where 6a–6c correspond to the moment when the robot turns the object around one of the corners of the ellipse using a sliding motion, and 6d–6f correspond to the moment when the robot recovers from a disturbance. In

the accompanying video, we also show the MPC modestly handling dynamic obstacles. Due to its short sighted TH—only 1 s—it only reacts when the obstacle is imminent.

D. Robot Experiment — Planning

In the final experiment, we demonstrate both planning a trajectory with obstacles and tracking that trajectory using the proposed MPCC formulation. The planning TH was $T = 22 \text{ s}$. Fig. 4g shows both the planning and the tracking trajectories for both the slider and the pusher. This experiment exemplifies the flexibility of our MPCC formulation, which is able to both plan and control the non-holonomic pusher-slider system—just by adjusting the TH of the problem.

V. SUMMARY AND DISCUSSION

This paper presents a Mathematical Program with Complementarity Constraints (MPCC) formulation for generating hybrid trajectories for planar pushing manipulation tasks. We show that this formulation is able to: (i) plan trajectories that exploit both sticking and sliding contact modes in scenarios with obstacles, and (ii) track nominal trajectories, using an MPC loop, under external disturbances and model uncertainties. We compare the proposed MPCC formulation with the mixed integer alternatives, *i.e.* with MINLP for planning trajectories and MIQP for control, showing that our formulation is i) computationally faster for planning problems, ii) computationally more reliable across different scenarios, iii) and better able to track challenging nominal trajectories and recover from disturbances. Furthermore, we tested our planner and MPC implementation on a KUKA LWR robot setup without any model identification, which demonstrates the reliability of the proposed controller.

This work demonstrates the potential of using complementarity constraints within an MPC for planar manipulation tasks involving contacts with friction. It remains to study the scalability of such approach with respect to number of contacts and different tasks, such as pivoting or non quasi-static scenarios. For future work, we will focus on improving the tracking performance via model selection and identification. Additionally, we aim to improve the MPC computation times towards increasing the time horizon, making it less short-sighted, and enabling its deployment in environments with highly dynamic obstacles.

ACKNOWLEDGMENT

This research is supported by the EU H2020 projects Enhancing Healthcare with Assistive Robotic Mobile Manip-

ulation (HARMONY, 101017008) and Memory of Motion (MEMMO, 780684), and the Kawada Robotics Corporation.

REFERENCES

- [1] M. T. Mason, "Mechanics and planning of manipulator pushing operations," *The International Journal of Robotics Research (IJRR)*, vol. 5, no. 3, 1986. DOI: 10.1177/027836498600500303.
- [2] F. R. Hogan and A. Rodriguez, "Reactive planar non-prehensile manipulation with hybrid model predictive control," *International Journal of Robotics Research (IJRR)*, vol. 39, no. 7, 2020. DOI: 10.1177/0278364920913938.
- [3] J. Zhou, R. Paolini, A. M. Johnson, J. A. Bagnell, and M. T. Mason, "A probabilistic planning framework for planar grasping under uncertainty," *IEEE Robotics and Automation Letters (RA-L)*, vol. 2, no. 4, 2017. DOI: 10.1109/LRA.2017.2720845.
- [4] M. Bauza and A. Rodriguez, "A probabilistic data-driven model for planar pushing," in *IEEE International Conference on Robotics and Automation (ICRA)*, 2017. DOI: 10.1109/ICRA.2017.7989345.
- [5] F. R. Hogan, E. R. Grau, and A. Rodriguez, "Reactive planar manipulation with convex hybrid mpc," in *IEEE International Conference on Robotics and Automation (ICRA)*, 2018. DOI: 10.1109/ICRA.2018.8461175.
- [6] M. Toussaint, K. R. Allen, K. A. Smith, and J. B. Tenenbaum, "Differentiable physics and stable modes for tool-use and manipulation planning - extended abstract," in *IJCAI International Joint Conference on Artificial Intelligence*, 2019. DOI: 10.24963/ijcai.2019/869.
- [7] T. Stouraitis, I. Chatz Nikolaidis, M. Gienger, and S. Vijayakumar, "Online hybrid motion planning for dyadic collaborative manipulation via bilevel optimization," *IEEE Transactions on Robotics*, vol. 36, no. 5, 2020. DOI: 10.1109/TRO.2020.2992987.
- [8] M. Toussaint, J. S. Ha, and D. Driess, "Describing physics for physical reasoning: Force-based sequential manipulation planning," *IEEE Robotics and Automation Letters (RA-L)*, vol. 5, no. 4, 2020. DOI: 10.1109/LRA.2020.3010462.
- [9] A. Aydinoglu, V. M. Preciado, and M. Posa, "Contact-aware controller design for complementarity systems," in *IEEE International Conference on Robotics and Automation (ICRA)*, 2020. DOI: 10.1109/ICRA40945.2020.9197568.
- [10] M. T. Mason, "Progress in nonprehensile manipulation," *International Journal of Robotics Research (IJRR)*, vol. 18, no. 11, 1999. DOI: 10.1177/02783649922067762.
- [11] S. Goyal, A. Ruina, and J. Papadopoulos, "Limit surface and moment function descriptions of planar sliding," in *IEEE International Conference on Robotics and Automation (ICRA)*, 1989. DOI: 10.1109/robot.1989.100081.
- [12] N. Chavan-Daffe, R. Holladay, and A. Rodriguez, "Planar in-hand manipulation via motion cones," *International Journal of Robotics Research (IJRR)*, vol. 39, no. 2-3, 2020. DOI: 10.1177/0278364919880257.
- [13] K. M. Lynch, H. Maekawa, and K. Tanie, "Manipulation and active sensing by pushing using tactile feedback," in *IEEE/RSJ International Conference on Intelligent Robots and Systems (IROS)*, vol. 1, 1992. DOI: 10.1109/IROS.1992.587370.
- [14] J. Zhou, R. Paolini, J. A. Bagnell, and M. T. Mason, "A convex polynomial force-motion model for planar sliding: Identification and application," in *IEEE International Conference on Robotics and Automation (ICRA)*, vol. 2016-June, IEEE, 2016, pp. 372-377. DOI: 10.1109/ICRA.2016.7487155.
- [15] T. Stouraitis, I. Chatz Nikolaidis, M. Gienger, and S. Vijayakumar, "Dyadic collaborative manipulation through hybrid trajectory optimization," in *Conference on Robot Learning (CoRL)*, vol. 87, 2018.
- [16] A. O. Onol, P. Long, and T. Padir, "Contact-implicit trajectory optimization based on a variable smooth contact model and successive convexification," in *IEEE International Conference on Robotics and Automation (ICRA)*, 2019. DOI: 10.1109/ICRA.2019.8794250.
- [17] J. P. Sleiman, J. Carius, R. Grandia, M. Wermelinger, and M. Hutter, "Contact-implicit trajectory optimization for dynamic object manipulation," in *IEEE International Conference on Intelligent Robots and Systems (IROS)*, 2019. DOI: 10.1109/IROS40897.2019.8968194.
- [18] M. Posa, C. Cantu, and R. Tedrake, "A direct method for trajectory optimization of rigid bodies through contact," *International Journal of Robotics Research (IJRR)*, vol. 33, no. 1, 2014. DOI: 10.1177/0278364913506757.
- [19] T. Stouraitis, L. Yan, J. Moura, M. Gienger, and S. Vijayakumar, "Multi-mode trajectory optimization for impact-aware manipulation," in *IEEE International Conference on Intelligent Robots and Systems (IROS)*, 2020. DOI: 10.1109/IROS45743.2020.9341246.
- [20] R. D. Howe and M. R. Cutkosky, "Practical force-motion models for sliding manipulation," *International Journal of Robotics Research (IJRR)*, vol. 15, no. 6, 1996. DOI: 10.1177/027836499601500603.
- [21] F. R. Hogan and A. Rodriguez, "Feedback control of the pusher-slider system: A story of hybrid and underactuated contact dynamics," in *Algorithmic Foundations of Robotics XII*, vol. 13, Springer International Publishing, 2020. DOI: 10.1007/978-3-030-43089-4_51.
- [22] G. L. Nemhauser and L. A. Wolsey, *Integer and Combinatorial Optimization*. Wiley-Interscience, 1988. DOI: 10.1002/9781118627372.
- [23] A. Nurkanovic, S. Albrecht, and M. Diehl, "Limits of mpcc formulations in direct optimal control with nonsmooth differential equations," in *European Control Conference (ECC)*, 2020. DOI: 10.23919/ecc51009.2020.9143593.
- [24] J. A. Andersson, J. Gillis, G. Horn, J. B. Rawlings, and M. Diehl, "Casadi: A software framework for nonlinear optimization and optimal control," *Mathematical Programming Computation*, vol. 11, no. 1, 2019. DOI: 10.1007/s12532-018-0139-4.
- [25] R. H. Byrd, J. Nocedal, and R. A. Waltz, "Knitro: An integrated package for nonlinear optimization," in *Large-Scale Nonlinear Optimization*, G. Di Pillo and M. Roma, Eds., Springer US, 2006. DOI: 10.1007/0-387-30065-1_4.
- [26] Gurobi Optimization, LLC, *Gurobi Optimizer Reference Manual*, 2021. [Online]. Available: <https://www.gurobi.com>.